# Characterization of a Novel, Magnetic Resonance Imaging-Compatible Rodent Model Spinal Cord Injury Device

## Tim Bhatnagar[1]
Department of Mechanical Engineering,
University of British Columbia,
Vancouver, BC V6T 1Z4, Canada;
International Collaboration
on Repair Discoveries (ICORD),
Vancouver, BC V5Z 1M9, Canada
e-mail: tim.bhatnagar@gmail.com

## Jie Liu
Department of Zoology, University of British Columbia,
Vancouver, BC V6T 1Z4, Canada;
International Collaboration
on Repair Discoveries (ICORD),
Vancouver, BC V5Z 1M9, Canada

## Thomas Oxland
Departments of Orthopaedics and Mechanical Engineering,
University of British Columbia,
Vancouver, BC V6T 1Z4, Canada;
International Collaboration on
Repair Discoveries (ICORD),
Vancouver, BC V5Z 1M9, Canada

*Rodent models of acute spinal cord injury (SCI) are often used to investigate the effects of injury mechanism, injury speed, and cord displacement magnitude, on the ensuing cascade of biological damage in the cord. However, due to its small size, experimental observations have largely been limited to the gross response of the cord. To properly understand the relationship between mechanical stimulus and biological damage, more information is needed about how the constituent tissues of the cord (i.e., gray and white matter) respond to injurious stimuli. To address this limitation, we developed a novel magnetic resonance imaging (MRI)-compatible test apparatus that can impose either a contusion-type or dislocation-type acute cervical SCI in a rodent model and facilitate MR-imaging of the cervical spinal cord in a 7 T MR scanner. In this study, we present the experimental performance parameters of the MR rig. Utilizing cadaveric specimens and static radiographs, we report contusion magnitude accuracy that for a desired 1.8 mm injury, a nominal 1.78 mm injury (SD = 0.12 mm) was achieved. High-speed video analysis was employed to determine the injury speeds for both mechanisms and were found to be 1147 mm/s (SD = 240 mm/s) and 184 mm/s (SD = 101 mm/s) for contusion and dislocation injuries, respectively. Furthermore, we present qualitative pilot data from a cadaveric trial, employing the MR rig, to show the expected results from future studies.* [DOI: 10.1115/1.4027670]

*Keywords: spinal cord injury, rodent model, MRI, injury mechanism, biomechanics*

## Introduction

The biomechanical response of the spinal cord to a mechanical insult is often studied using a rodent animal model [1–4]. A number of devices reported in the literature can accurately create repeatable spinal cord injuries (SCIs) in rodent models (e.g., UBC machine [5], Infinite horizon [6], NYU impactor [7], OSU machine [8]). These existing SCI devices have facilitated the measurement of force and displacement of the spinal cord during injury. These devices have also provided consistent injury models to investigate the biological damage response from the spinal cord and thereby provide a platform on which to evaluate the effectiveness of neuro-therapeutic or neural repair strategies.

Researchers have used these models, previously, to investigate various mechanical parameters of acute SCI. Kearney et al. suggested the product of impact velocity and relative cord compression to indicate a threshold of injury severity, with respect to recovery of neurological function in a ferret model [9]. Sparrey et al. investigated the effects of different contusion speeds (3 mm/s and 300 mm/s) in a rodent model, finding that hemorrhage in the white matter, and damage to the neurons and dendrites in the gray matter significantly increased with higher impact velocities [10]. Choo et al. showed distinct differences in spinal cord biological response when different SCI mechanisms were induced on the rodent spinal cord; specifically, the clinically relevant injury mechanisms of contusion, dislocation, and distraction had damage patterns that were easily differentiable, confirming that different injury mechanisms lead to different patterns of spinal cord damage [5].

While existing experimental models have facilitated mechanical measures of spinal cord response during SCI, the data obtained are restricted to describing the force-response and displacement of the gross cord (i.e., white matter and gray matter surrounded by the meninges of the spinal cord). The difference in material properties of the meninges [11–13] and the white and gray matters [14–16] suggests that the cord is a heterogeneous body. To further understand the relationship between spinal cord deformation and the pattern of ensuing biological damage, a more localized, comprehensive measure of spinal cord motion during injury is required.

Computational models of SCI have also been developed to elucidate the deformations of the spinal cord due to contusion, dislocation, and distraction injuries [17,18]. Most recently, it was shown that maximum principal strain correlates well with local tissue damage in contusion or dislocation injuries, using a computational model [18]. A current limitation on all computational models of the spinal cord is that there is no generally agreed upon set of material values to be used. Although there have been attempts to experimentally quantify the parenchymal tissue mechanical properties [2,14,16,19–21], the variations of the measurement technique, state of the tissue (i.e., in vivo, fixed, cadaveric, etc), species from which the sample was obtained and complexity of material model utilized among published studies make comparisons and consensus determination difficult. Sparrey et al. studied the effects of varying material properties in a computational SCI model, showing that stresses and pressures within the cord vary substantially during static compression when different literature-reported tissue properties are used in the model [22]. While computational modeling does further the study of acute SCI, a method to obtain experimental data of the morphology of spinal cord parenchymal tissues due to injury would improve the models by providing data for validation. To provide an internal set of measurements of the spinal cord during acute SCI, we propose to use MRI methods to differentiate between white and gray matter deformation in the spinal cord during sustained contusion and dislocation injuries.

Recently, MRI methods have been used more frequently for visualizing the spinal cord, both in clinical cases [23–25] and in research models [26–30]. MR images of the rat spinal cord can be segmented into gray and white matter using an in vivo, noninvasive method [29,30]. Therefore, there is potential to quantify internal spinal cord deformation due to SCI, using pre-injury and
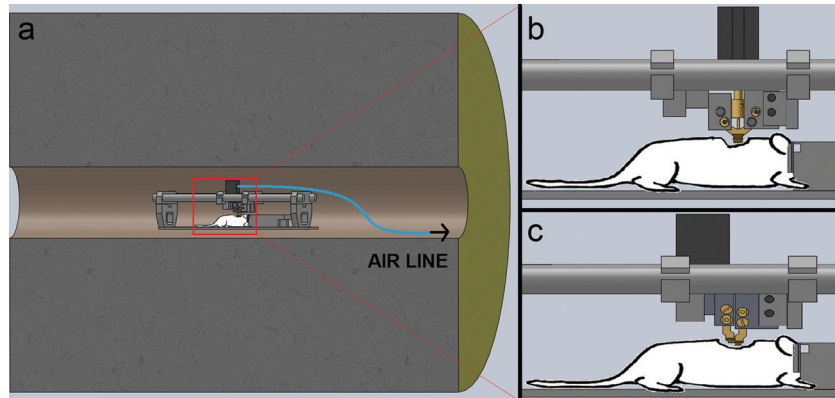
**Fig. 1 The novel MR rig. (a)** For MR image acquisition, the specimen is loaded into the MR rig and is placed at the center of the bore of the MR scanner—represented by the cylindrical cut-away. The "air line" (blue) supplies the pneumatic actuator (dark gray) with pressurized air from outside the MR scanner. The red box outlines the portion of the MR rig shown in (b) and (c); (b) the MR rig contusion configuration with clamps attached to the cervical spine of a specimen; (c) the MR rig dislocation configuration with clamps attached to the cervical spine of a specimen.

sustained-injury MR images. To accomplish this, a novel, pneumatic, MR-compatible, rodent model SCI device was designed (hereafter referred to as the "MR rig"). The device is capable of inducing either a contusion or dorsal dislocation injury, at variable severity, to the cervical spinal cord while inside the bore of a 7 T MR scanner. The goal of this study was to characterize the MR rig by showing its capability to produce cervical contusion and dislocation injuries in a rodent model with repeatable displacements and speeds such that it could be used in future studies to investigate SCI in a rodent model.

## Materials and Methods

The MR rig size, material selection, and mode of operation were designed to be compatible with a 7 T MRI scanner (Bruker Biospec, Germany). Two mechanisms of acute cervical SCI in a Sprague–Dawley rat model were possible in the MR rig: a dorsal contusion or a dorsal dislocation. Methods used to obtain the cadaveric specimen for experimentation were carried out according to protocols approved by the Animal Care Committee at the University of British Columbia. The MR rig was evaluated for precision of injury speed in both injury mechanisms with a 1.8 mm contusion injury and a 2.5 mm dislocation injury—these parameters were determined to be the maximal severity for each injury mechanism, in an in vivo Sprague–Dawley model that could be sustained for the duration of imaging and still have the animal survive. Due to the different mechanical actuation process of each injury mechanism (i.e., contusion and dislocation), measures of displacement accuracy and precision were made only for the contusion injury. The displacement for the dislocation mechanism was determined solely by the physical stroke length of the actuator and, therefore, did not require evaluation of accuracy or precision. The design, materials, and function of the MR rig, as well as the methods used to assess accuracy and precision, are presented. As an example of the images facilitated by the MR rig, preliminary results from experimental use of the MR rig are also presented for qualitative analysis.

The MR rig design geometry was restricted to the 7 T MR scanner with a bore diameter of 20 cm. MR-compatibility dictated that the device be made of nonmetals; the main body of the device was constructed from ultra high-molecular weight polyethylene. A custom plastic pneumatic actuator (BECO Manufacturing Co. Inc., Laguna Hills, CA) was used to actuate both the contusion and dislocation injury mechanisms. The inlet pneumatic line to the actuator was pressurized using an air compressor (100 psi rating, Campbell-Hausfeld). Additionally, the MR rig includes a stereotaxic frame and ear bars to ensure proper alignment of the

animal and a port-hole in the base plate to facilitate the delivery of gaseous anesthesia during the MR image acquisition period. To acquire optimal data, the MR rig needed to be placed in the MR scanner bore such that the region of interest (i.e., the cervical spinal cord) was situated at the center point of the MR scanner [Fig. 1(a)]. The MR rig was designed to create both cervical contusion and dislocation SCI at speeds and displacements similar to those outlined by Choo et al. (speeds: 998 mm/s and 956 mm/s, respectively; displacements: 1.1 mm and 2.5 mm, respectively) [5]. To facilitate each injury mechanism, the pneumatic actuator mounts and cervical spine interface components of the MR rig were designed to be modular and interchangeable [Figs. 1(b) and 1(c)].

The interface between the MR rig and the rodent spine was adopted and modified from the work by Choo et al. [5]. Vertebral clamps were designed to prevent motion of the spine and were constructed from polyether–ether–ketone because of its biocompatibility, stiffness, and high yield strength [31] (Fig. 2). The contusion clamps attached dorsally to the cervical spine via both vertebral lateral notches from the C4 to the C7 vertebral body (Fig. 3). To induce the contusion injury, the pneumatic actuator was activated to extend a piston with a 2 mm spherical contusion tip, ventrally into the spinal canal at a prescribed depth of 1.8 mm, via a laminectomy at the C5/6 level [Fig. 3(a)]. For the dislocation injury mechanism, the spinal clamps consisted of two sets—the cranial clamp set and the caudal clamp set (Fig. 4). The cranial clamps attached dorsally to the spine at the vertebral lateral notches of C4–C5, and the caudal clamps attached similarly at C6–C7. Both clamp sets used vertebral endplate teeth (positioned
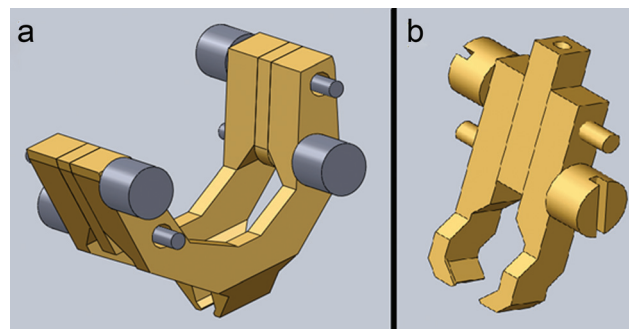


**Fig. 2 Custom designed spinal clamps to facilitate SCI. (a)** Custom contusion injury clamps; (b) one set of the pair of identical, custom dislocation clamps that are used to create a dislocation injury.
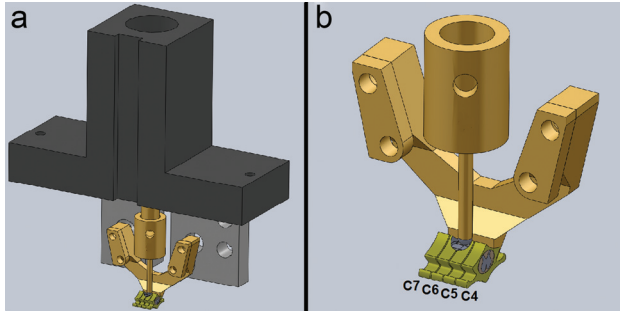
Fig. 3 Schematic diagram of the contusion injury. (*a*) The contusion clamps attach rigidly to the cervical spine and the laminectomy at C5/6 is centered beneath the contusion impactor, which is driven into the dorsal surface of the spinal cord by the pneumatic actuator (dark gray); (*b*) the contusion clamps attach to vertebrae C4–C7 via the lateral notches of the spine.



Fig. 5 Sample static X-ray images to determine contusion injury displacement magnitude. (*a*) The dorsoventral (DV) diameter of the spinal canal is measured (shown in red) and used as an approximate DV-diameter of the spinal cord; (*b*) the 2 mm spherical impactor is used as a gauge-length for pixel-mm measurement conversion; (*c*) once the contusion injury is actuated, a final X-ray is used to determine the remaining distance between the tip of the spherical impactor and the ventral wall of the spinal canal.

between C5 and C6) to resist motion in the axial direction. The dislocation was induced by activating the pneumatic actuator, which retracted the caudal clamp mounting block (rigidly linked to vertebrae C6–C7) dorsally, to a prescribed distance of 2.5 mm, while the cranial clamp (rigidly linked to vertebrae C4–C5) remained fixed [Figs. 4(*b*) and 4(*c*)].

### Contusion Evaluation

*Displacement.* The contusion injury consisted of an impact to the approximate midline of the dorsal surface of the spinal cord between C5 and C6, with a 2 mm sphere attached to an actuating arm [Fig. 5(*a*)]. Injury displacement in the contusion model was quantified as the amount of cord compression under the impacting sphere. To evaluate accuracy of a 1.8 mm injury, cadaveric C4–C7 cervical spinal columns ($n = 7$, Sprague–Dawley rats, approx. 300 g) were harvested and the spinal cords were removed from the spinal canals. A partial dorsal laminectomy was performed over the C5 and C6 vertebrae, and then the column was clamped into the MR rig. A static X-ray (70 kvP, 15 mA, 1/5 s duration, Mobile 100-15—GE) was then taken in the transverse plane such that the image (Fuji Computed Radiography Console Lite—FujiFilm, Japan) showed the spinal canal through the cervical vertebrae. The original 2 mm plastic sphere tip was replaced

with a 2 mm stainless steel ball bearing for this accuracy study to utilize the radio-opaqueness of the metal tip as a scaling reference. The contusion injury was then actuated, followed by another static X-ray with the same spatial resolution as the previous image, which showed the contusion impactor intruding into the spinal canal [Fig. 5(*c*)]. The "injured" X-ray image was then analyzed (ImageJ—NIH) to determine the pixel-mm conversion ratio, using the 2 mm steel sphere as a reference-length [Fig. 5(*b*)]; the distance between the tip of the spherical impactor and the ventral wall of the spinal canal was then determined. From the first "uninjured" X-ray, the pixel-mm ratio was used to determine the dorsoventral diameter of the spinal canal. The injury displacement magnitude was then calculated as the dorsoventral diameter of the spinal canal (from "uninjured" X-ray) minus the residual space between the impactor and the ventral wall of the canal (from "injured" X-ray). These measurements were made 3 times on every image by a single observer, which yielded a precision value (standard deviation) of approximately 0.22 mm.

*Speed.* The contusion displacement-time profiles were acquired for a range of pressures to determine the range of contusion speeds for the MR rig. The contusion injury speed was measured without a specimen in the MR rig since the spinal cord does not provide a large resistive force upon impact ($\sim 2$ N [5]); thus, a "blank" injury trial was assumed to yield the same injury speed as if there were a specimen present. A high-speed (HS) camera
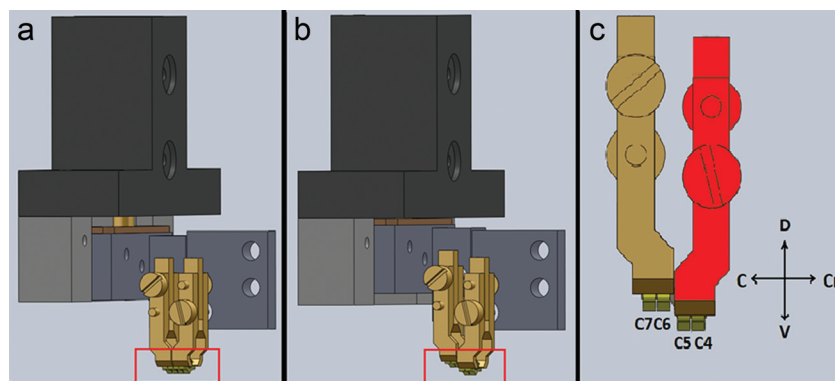


Fig. 4 Schematic diagram of the dislocation setup. (*a*) The caudal clamp mount links the caudal dislocation clamp (attached to C6–C7) to the actuating piston. The piston travel length (i.e., the dislocation magnitude—2.5 mm) is limited by the insertion of a spacing block (brown), between the caudal assembly and the pneumatic actuator (dark gray). The red box highlights the cervical spine linked to the apparatus; (*b*) actuation of the piston causes the caudal assembly to dorsally translate, relative to the fixed cranial assembly, until the spacing block prevents further motion; (*c*) a detailed view of the imposed dislocation injury with the cranial clamps (red) fixed and anatomical directions indicated: D—dorsal, V—ventral, C—caudal, Cr—cranial.
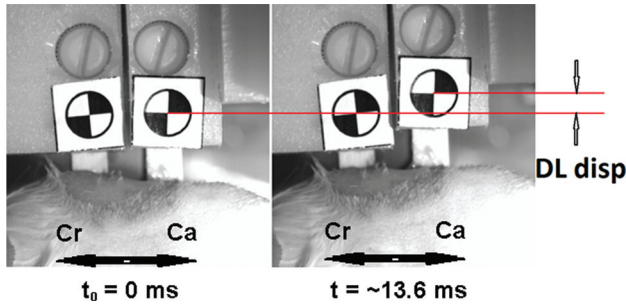
Fig. 6 Measurement of dislocation injury (DL) displacement using HS video. The displacement of the caudal set of clamps is tracked (left, initial position; right, final position—2.5 mm), and the average speed is determined by dividing the displacement by the time required to complete the injury (~13.6 ms). The cranial ("Cr") and caudal ("Ca") directions are indicated.

(3000 fps, $576 \times 576$ resolution, Phantom-Vision Research) was used to record the actuator stroke position throughout the contusion injury event; the camera had an assessed accuracy of 0.016 mm with precision (SD) of 0.01 mm. The stroke position was measured in the HS video by tracking a reference marker affixed to the contusion impactor. To determine the impact speed of a 1.8 mm contusion injury displacement at a given supplied air pressure, the displacement-time data were interpolated to find the actuator speed when the impactor tip was 1.8 mm from its maximum displacement, representative of the time at which the impactor would contact the spinal cord. During the contusion speed trials, a wide range of actuator inlet pressures was utilized (21–89 psi; $n = 27$); however, during experimentation only a higher subrange of inlet pressures (77–89 psi; $n = 14$) was used to achieve the highest speeds possible with the air compressor used. A regression analysis was performed to determine how the injury speed was related to the actuator pressure in the full pressure range, as well as the experimental working range.

**Dislocation Evaluation.** The dislocation injury consisted of a dorsal translation of the C6 vertebra with respect to the C5 vertebra (Fig. 4). Injury displacement in the dislocation model was representative of the actual distance that C6 was translated with respect to C5. C4–C5 and C6–C7 were rigidly attached to the cranial and caudal set of clamps, respectively. Due to this rigid attachment, the dislocation displacement magnitude was equivalent to the stroke length of the actuator, a manually set length, and neither accuracy nor precision were evaluated.

*Speed.* Different from the contusion injury speed trials, the dislocation injury speed was determined while cadaveric specimens were clamped into the MR rig, since a dislocation of the spinal column provides a greater resistance force (~20 N [5]) than the contusion injury. In order to evaluate the injury speed of a 2.5 mm injury, cadaveric C2–C8 cervical spinal columns ($n = 8$, Sprague–Dawley rats, approx. 300 g) were harvested for a dislocation injury. A facetectomy was performed on either side of the C5/C6 vertebral junction, and the spine was then clamped into the MR device. Initial alignment of the cranial and caudal clamps was determined by sight to ensure no pre-injury dislocation was induced. The injury was then actuated and high-speed video (3000 fps, $576 \times 576$ resolution) was used to track the motion of the dislocation injury clamps using the reference markers affixed on each clamp (Fig. 6). The pixel-mm conversion was based on the reference markers (6.35 mm diameter), and the displacement of the caudal clamps during the injury, in millimeters, was calculated. The average dislocation injury speed was determined by dividing the total dislocation displacement by the time interval required for the injury. During the dislocation speed trials, a range of actuator inlet pressures was utilized (79–89 psi; $n = 8$). A regression analysis was performed to
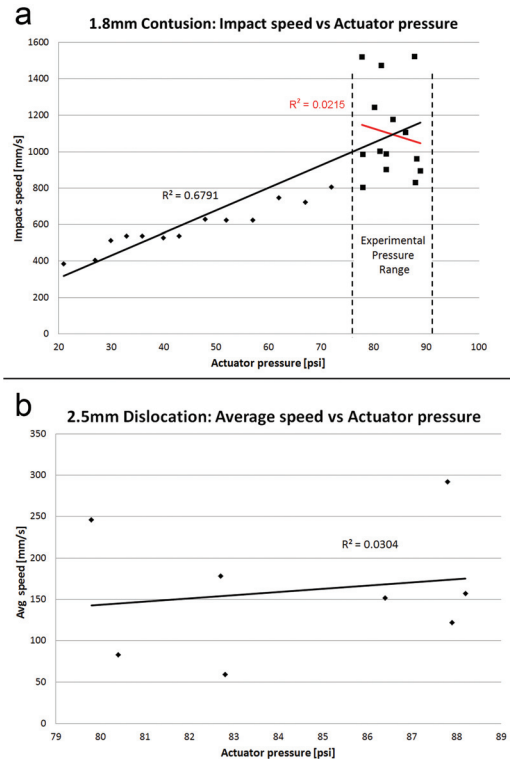


Fig. 7 Injury speeds as a function of actuator inlet pressure. (*a*) Regression analysis of the contusion injury impact speed against actuator inlet pressure shows a relationship over a wide pressure range [$R_1^2$ (black); 21–88 psi] but no discernible relationship within the experimental pressure range [$R_2^2$ (red); 78–88 psi]; (*b*) the same analysis for average dislocation injury speed against actuator inlet pressure indicated that within the pressure ranges specified, the change in inlet pressure did not have a predictable effect on the injury speeds.
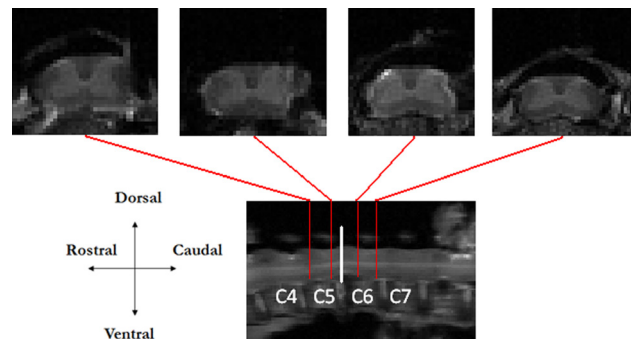


Fig. 8 Sample images using the MR rig—pre-injury. The MR rig facilitates imaging of the in vivo rodent spinal cord, with differentiation between the white and the gray matter of the cord. Sample cross-sectional slices are shown from different parts of the cord along the intended injury area (marked by the white, solid line in the sagittal view image).

determine how the injury speed was related to the actuator pressure in the pressure range tested.

## Results

The accuracy of the MR rig contusion injury was determined by quantifying the mean and standard deviation of the actuator tip displacement during an intended 1.8 mm injury. The average contusion injury displacement was determined to be 1.78 mm (SD 0.12 mm). The intended speed for both the contusion and
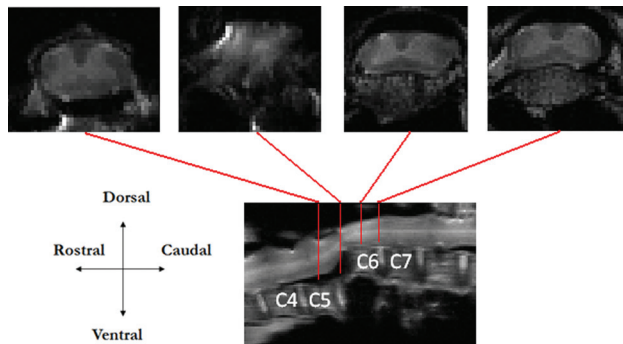
**Fig. 9 Sample images using the MR rig—during injury. The 2.5 mm dislocation injury is easily visualized in the sagittal view. The representative cross-sectional slices (taken from the same levels as in the pre-injury scan) clearly show local deformation of the white and gray matter due to the dislocation injury.**

dislocation injuries was approximately 1000 mm/s, based upon previous work [5]. The impact speed for a 1.8 mm contusion injury was determined to be 1100 mm/s (SD 250 mm/s). The average dislocation speed for a 2.5 mm injury was determined to be 184 mm/s (SD 101 mm/s).

Contusion impact speed was plotted against actuator inlet pressure. Using a regression analysis, it can be seen that there is a relationship within the tested range pneumatic actuator inlet pressures (21–88 psi) and the instantaneous injury speed for a 1.8 mm contusion [$R_1^2 = 0.6791$, Fig. 7(a)]. However, in the experimental working range of actuator inlet pressures (79–89 psi), there was no observable relationship between injury speed and inlet pressure [$R_2^2 = 0.0215$, Fig. 7(a)], with an injury speed range of 805–1505 mm/s. Similarly, average dislocation speed for a 2.5 mm injury was plotted against actuator inlet pressure and did not yield a significant correlation [$R^2 = 0.0304$, Fig. 7(b)], with an injury speed range of 61–292 mm/s. A wider pressure-speed profile was not obtained for the dislocation injury mechanism; dislocation speed tests required use of a cadaveric specimen, which were limited in availability. We would expect a similar trend of decreasing dislocation injury speeds with decreasing actuator inlet pressures.

The resultant MR images (T$_2$ spin-echo sequence, $140 \times 140$ $\mu$m in-plane resolution, 500 $\mu$m slice, ~30 min acquisition time) acquired during an experimental 2.5 mm dislocation injury in a Sprague–Dawley cadaveric model are shown in Figs. 8 (pre-injury) and 9 (sustained-injury). There is excellent differentiation between the white and gray matter of the spinal cord, and a distinct pattern of deformation is easily observed when a 2.5 mm dislocation injury is performed inside the 7 T MR scanner.

## Discussion

The goal of this study was to verify that the novel MR rig is capable of producing cervical contusion and dislocation injuries in a rodent model with repeatable displacements and speeds such that it could be used in future studies to investigate SCI in a rodent model. The MR rig was characterized in terms of contusion and dislocation injury speed (both functions of the supplied air pressure), as well as contusion accuracy (evaluated for a 1.8 mm injury). Dislocation accuracy was not specifically addressed as the MR rig design ensured the desired amount of actuator stroke travel was achieved.

Although the model of SCI in a rodent developed by Choo et al. provides a better measure of accuracy (i.e., contusion injury speed SD: 37 mm/s; dislocation speed SD: 32 mm/s) [5], the MR rig is the first apparatus that can be used to perform SCI experiments inside of an MR scanner. Conducting the entire experiment within the MR scanner without removal or repositioning is highly desirable because it removes the possibility of errors being

introduced into the system from motion of the apparatus or the specimen and it ensures correct global alignment between image sets. Additionally, it is possible to determine contusion and dislocation displacement magnitudes from the MR images that are acquired when using this device such that any errors in the MR rig injury magnitudes can be monitored during experimentation.

With respect to the injury speeds produced by the MR rig, the contusion speed is comparable to that employed by Choo et al. [5], but the dislocation speed with the MR rig was considerably slower than Choo et al. This discrepancy is most likely caused by the larger force required to produce a dislocation injury compared to a contusion injury (i.e., ~20 N and ~2 N, respectively), which is due to the dynamic involvement of the intervertebral disk [5]. While there has been research to show that drastically different contusion injury speeds (differing by 2 orders of magnitude) in rodent model SCI produce statistically different outcomes of ensuing biological damage [10], the speeds achieved in the dislocation injury in this study were the maximum attainable based on the air-pump used.

Further investigation into the effect of injury speed (for both contusion and dislocation mechanisms, in the ranges utilized in this study) on damage to the spinal cord would help to determine if the MR rig is producing a drastically different injury than that developed by Choo et al. [5].

Due to constraints for MR-compatibility, stiff plastics were used for the construction of the MR rig instead of more rigid metals. During dislocation experiments, it was observed that there was slight motion of the cranial clamps (and therefore motion of the C5 vertebrae), which could have the effect of reducing the true displacement of C6 with respect to C5. Both injury mechanism speeds showed considerable amount of variability; for both mechanisms, the pneumatic actuator may introduce variability based on the lubrication state of the stroke piston or the integrity of the gaskets containing the pressurized air. While there is a clear relationship between actuator inlet pressure and injury speed over a wide range of pressures, within the pressure range used experimentally there was no observable difference in the speeds produced by the actuator. The high-range of pressure (79–89 psi) was used to facilitate the highest speeds possible to try and replicate the experiments performed by Choo et al. [5]. The variability of the average dislocation injury speed was larger than the variability of the contusion impact speed, indicating that involvement of more of the spinal column complex during injury (spinal ligaments, intervertebral disk, etc.) may result in decreased precision of injury speed due to anatomical variation. Based on the reported effects of injury speed on ensuing damage in SCI contusion models [10], a further-refined pneumatic actuator device capable of achieving higher injury speed precision with a given inlet pressure would be a worthwhile improvement in this model. Measurements for contusion injury displacement were also susceptible to limitations of the X-ray based data; the pixel-mm conversion factor was based on the 2 mm-diameter ball bearing which showed slight blurriness at its edges, making repeatable measures of the gauge-length difficult. Since the precision of the X-ray based measurements, 0.22 mm, was larger than the accuracy parameter for the same measurements, 0.12 mm, it may be useful to employ higher resolution image data or postprocessing methods that would reduce intra-observer variability. Additionally, the dorsoventral diameter of the spinal cord was assumed to be equal to that of the spinal canal at the same level; qualitatively, it was noted that there may be some discrepancy between these two-dimensions, but a more accurate measure of specimen-specific spinal cord diameter was not able to be determined. Lastly, the regression analysis of each injury mechanism speed as a function of actuator pressure indicated that there may be factors in the injury process that have not yet been accounted for. A more thorough understanding of how the injury speed and pressure are related, in this model, may be ascertained by experimenting with a wider range of inlet pressures, as well as investigating the utilization of a more refined pneumatic actuator.

Although a number of limitations have been identified in the performance of the MR rig, the sample images from preliminary,

cadaveric experimental use (Figs. 8 and 9) show observations of SCI that have never been possible previously with other SCI models. Experimentation using the MR rig will be able to provide data that can be quantified to determine how the spinal cord deforms internally, whereas previous SCI models have only been able to measure gross cord deformation. The ability to observe the internal aspects of the spinal cord during injury is crucial to understanding the biomechanics of the cord during an SCI event. Quantifiable deformation data would be able to be integrated into computational models to increase the level of biofidelity as well as establish thresholds of deformation-based injury for the substructures of the spinal cord (i.e., the white and gray matter). The development of this MR rig provides internal spinal cord deformation data that have not been attainable previously and will be useful in furthering models of in vivo rodent SCI.

## References

[1] Choo, A. M., Liu, J., Lam, C. K., Dvorak, M., Tetzlaff, W., and Oxland, T. R., 2007, "Contusion, Dislocation, and Distraction: Primary Hemorrhage and Membrane Permeability in Distinct Mechanisms of Spinal Cord Injury," J. Neurosurg.: Spine, 6(3), pp. 255–266.

[2] Fiford, R. J., and Bilston, L. E., 2005, "The Mechanical Properties of Rat Spinal Cord in vitro," J. Biomech., 38(7), pp. 1509–1515.

[3] Maikos, J. T., and Shreiber, D. I., 2007, "Immediate Damage to the Blood-Spinal Cord Barrier Due to Mechanical Trauma," J. Neurotrauma, 24(3), pp. 492–507.

[4] Maikos, J. T., Qian, Z., Metaxas, D., and Shreiber, D. I., 2008, "Finite Element Analysis of Spinal Cord Injury in the Rat," J. Neurotrauma, 25(7), pp. 795–816.

[5] Choo, A. M., Liu, J., Liu, Z., Dvorak, M., Tetzlaff, W., and Oxland, T. R., 2009, "Modeling Spinal Cord Contusion, Dislocation, and Distraction: Characterization of Vertebral Clamps, Injury Severities, and Node of Ranvier Deformations," J. Neurosci. Methods, 181(1), pp. 6–17.

[6] Scheff, S. W., Rabchevsky, A. G., Fogaccia, I., Main, J. A., and Lumpp, J. E., Jr., 2003, "Experimental Modeling of Spinal Cord Injury: Characterization of a Force-Defined Injury Device," J. Neurotrauma, 20(2), pp. 179–193.

[7] Gruner, J. A., 1992, "A Monitored Contusion Model of Spinal Cord Injury in the Rat," J. Neurotrauma, 9(2), pp. 123–126.

[8] Noyes, D. H., 1987, "Electromechanical Impactor for Producing Experimental Spinal Cord Injury in Animals," Med. Biol. Eng. Comput., 25(3), pp. 335–340.

[9] Kearney, P. A., Ridella, S. A., Viano, D. C., and Anderson, T. E., 1988, "Interaction of Contact Velocity and Cord Compression in Determining the Severity of Spinal Cord Injury," J. Neurotrauma, 5(3), pp. 187–208.

[10] Sparrey, C. J., Choo, A. M., Liu, J., Tetzlaff, W., and Oxland, T. R., 2008, "The Distribution of Tissue Damage in the Spinal Cord is Influenced by the Contusion Velocity," Spine, 33(22), pp. E812–E819.

[11] Jin, X., Lee, J. B., Leung, L. Y., Zhang, L., Yang, K. H., and King, A. I., 2006, "Biomechanical Response of the Bovine Pia-Arachnoid Complex to Tensile Loading at Varying Strain-Rates," Stapp Car Crash J., 50, pp. 637–649.

[12] Maikos, J. T., Elias, R. A., and Shreiber, D. I., 2008, "Mechanical Properties of Dura Mater From the Rat Brain and Spinal Cord," J. Neurotrauma, 25(1), pp. 38–51.

[13] Ozawa, H., Matsumoto, T., Ohashi, T., Sato, M., and Kokubun, S., 2004, "Mechanical Properties and Function of the Spinal Pia Mater," J. Neurosurg.: Spine, 1(1), pp. 122–127.

[14] Ichihara, K., Taguchi, T., Shimada, Y., Sakuramoto, I., Kawano, S., and Kawai, S., 2001, "Gray Matter of the Bovine Cervical Spinal Cord is Mechanically More Rigid and Fragile Than the White Matter," J. Neurotrauma, 18(3), pp. 361–367.

[15] Ichihara, K., Taguchi, T., Sakuramoto, I., Kawano, S., and Kawai, S., 2003, "Mechanism of the Spinal Cord Injury and the Cervical Spondylotic Myelopathy: New Approach Based on the Mechanical Features of the Spinal Cord White and Gray Matter," J. Neurosurgery, 99(3), pp. 278–285.

[16] Ozawa, H., Matsumoto, T., Ohashi, T., Sato, M., and Kokubun, S., 2001, "Comparison of Spinal Cord Gray Matter and White Matter Softness: Measurement by Pipette Aspiration Method," J. Neurosurg., 95(2), pp. 221–224.

[17] Greaves, C. Y., Gadala, M. S., and Oxland, T. R., 2008, "A Three-Dimensional Finite Element Model of the Cervical Spine With Spinal Cord: An Investigation of Three Injury Mechanisms," Ann. Biomed. Eng., 36(3), pp. 396–405.

[18] Russell, C. M., Choo, A. M., Tetzlaff, W., Chung, T. E., and Oxland, T. R., 2012, "Maximum Principal Strain Correlates With Spinal Cord Tissue Damage in Contusion and Dislocation Injuries in the Rat Cervical Spine," J. Neurotrauma, 29(8), pp. 1574–1585.

[19] Bilston, L. E., and Thibeault, L. E., 1996, "The Mechanical Properties of the Human Spinal Cord in vitro," Ann. Biomed. Eng., 24, pp. 67–74.

[20] Cheng, S., Clarke, E. C., and Bilston, L. E., 2008, "Rheological Properties of the Tissues of the Central Nervous System: A Review," Med. Eng. Phys., 30, pp. 1318–1337.

[21] Sparrey, C. J., and Keaveny, T. M., 2011, "Compression Behavior of Porcine Spinal Cord White Matter," J. Biomech., 44, pp. 1078–1082.

[22] Sparrey, C. J., Manley, G. T., and Keaveny, T. M., 2009, "Effects of White, Grey, and Pia Mater Properties on Tissue Level Stresses and Strains in the Compressed Spinal Cord," J. Neurotrauma, 26(4), pp. 585–595.

[23] Cheran, S., Shanmuganathan, K., Zhuo, J., Mirvis, S. E., Aarabi, B., Alexander, M. T., and Gullapalli, R. P., 2011, "Correlation of MR Diffusion Tensor Imaging Parameters With ASIA Motor Scores in Hemorrhagic and Nonhemorrhagic Acute Spinal Cord Injury," J. Neurotrauma, 28(9), pp. 1881–1892.

[24] Fehlings, M. G., Cadotte, D. W., and Fehlings, L. N., 2011, "A Series of Systematic Reviews on the Treatment of Acute Spinal Cord Injury: A Foundation for Best Medical Practice," J. Neurotrauma, 28(8), pp. 1329–1333.

[25] Parashari, U. C., Khanduri, S., Bhadury, S., Kohli, N., Parihar, A., Singh, R., Srivastava, R. N., and Upadhyay, D., 2011, "Diagnostic and Prognostic Role of MRI in Spinal Trauma, its Comparison and Correlation With Clinical Profile and Neurological Outcome, According to ASIA Impairment Scale," J. Craniovertebr. Junction Spine, 2(1), pp. 17–26.

[26] Ellingson, B. M., Schmit, B. D., and Kurpad, S. N., 2010, "Lesion Growth and Degeneration Patterns Measured Using Diffusion Tensor 9.4-T Magnetic Resonance Imaging in Rat Spinal Cord Injury," J. Neurosurg.: Spine, 13(2), pp. 181–192.

[27] Gonzalez-Lara, L. E., Xu, X., Hofstretova, K., Pniak, A., Brown, A., and Foster, P. J., 2009, "In vivo Magnetic Resonance Imaging of Spinal Cord Injury in the Mouse," J. Neurotrauma, 26(5), pp. 753–762.

[28] Kim, J. H., Loy, D. N., Wang, Q., Budde, M. D., Schmidt, R. E., Trinkaus, K., and Song, S. K., 2010, "Diffusion Tensor Imaging at 3 Hours After Traumatic Spinal Cord Injury Predicts Long-Term Locomotor Recovery," J. Neurotrauma, 27(3), pp. 587–598.

[29] Kozlowski, P., Raj, D., Liu, J., Lam, C., Yung, A. C., and Tetzlaff, W., 2008, "Characterizing White Matter Damage in Rat Spinal Cord With Quantitative MRI and Histology," J. Neurotrauma, 25(6), pp. 653–676.

[30] Yung, A. C., and Kozlowski, P., 2007, "Signal-to-Noise Ratio Comparison of Phased-Array vs. Implantable Coil for Rat Spinal Cord MRI," Magn. Reson. Imaging, 25(8), pp. 1215–1221.

[31] Kurtz, S. M., and Devine, J. N., 2007, "PEEK Biomaterials in Trauma, Orthopedic, and Spinal Implants," Biomaterials, 28(32), pp. 4845–4869.